Analyst

Accepted Manuscript

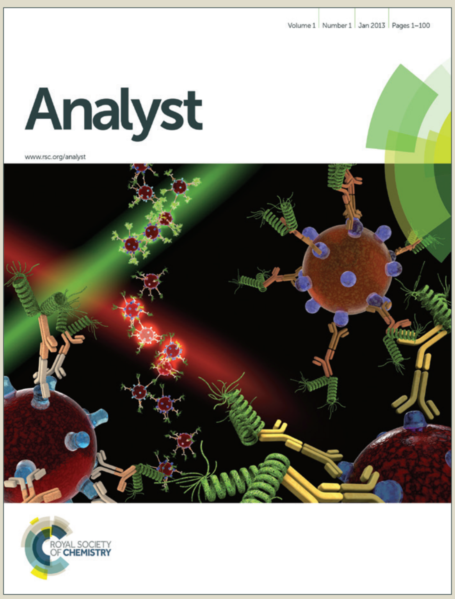

Ion Collision Cross Section Measurements in Quadrupole Ion Traps Using a Time-frequency Analysis Method

Muyi He,[1] Dan Guo,[1] Yu Chen,[2] Xingchuang Xiong,[3] Xiang Fang[3] and Wei Xu[1*]

[1]School of Life Science, Beijing Institute of Technology, Beijing 100081, China

[2]Shanxi Cancer Hospital, Xian, Shanxi 710061, China

[3]National Institute of Metrology, Beijing 100013, China

*Corresponding Author:
Wei Xu
School of Life Science
Beijing Institute of Technology
Haidian, Beijing, 100081, China
Email: weixu@bit.edu.cn
Phone: +86-10-68918123

Abstract

In this study, a method for measuring ion collision cross sections (CCSs) was proposed through time-frequency analysis of ion trajectories in quadrupole ion traps. A linear ion trap with added high-order electric fields was designed and simulated. With the presence of high-order electric fields and ion-neutral collisions, ion secular motion frequency within the quadrupole ion trap will be a function of ion motion amplitude, thus a function of time and ion CCS. A direct relationship was then established between ion CCS and ion motion frequency with respect to time, which could be obtained through time-frequency analysis of ion trajectories (or ion motion induced image currents). To confirm the proposed theory, realistic ion trajectory simulations were performed, where the CCSs of bradykinin, angiotensin I and II, ubiquitin ions were calculated from simulated ion trajectories. As an example, differentiation of isomeric ubiquitin ions was also demonstrated in simulations.

Key words: collision cross section; time-frequency analysis; linear ion trap; high-order field; ion-neutral collision; isomer.

1. Introduction

Ion structure analysis is an important topic in mass spectrometry (MS), especially during the analyses of biomolecules. Structural analyses of proteins are critically important for understanding their biological functions. Up to now, tandem MS techniques, such as collision induced dissociation (CID),[1-3] electron transfer dissociation (ETD)[4-6] and electron capture dissociation (ECD),[7-10] have been developed and widely applied in proteomics for the analyses of peptide mass fingerprint (PMF) and post-translational modifications (PTM). Nevertheless, identifying ions with the same mass-to-charge ratio (m/z) but different structures such as isomers, stable conformers and protein complexes with multi-conformations, are still challenging topics. Ion collision cross section (CCS) measurements with ion mobility spectrometry (IMS) techniques have also been applied as a complementary method to study ion structure.[11-17]

To measure the CCS of an ion, several instruments and techniques have been developed, such as drift-time ion mobility spectrometry (DTIMS)[18], differential-mobility spectrometry (DMS)[19], high-field asymmetric waveform ion mobility spectrometry (FAIMS)[20] and traveling wave ion mobility spectrometry (TWIMS).[21] During an IMS experiment, it is necessary to pay attention to ion fragmentations or conformation variations caused by high-energy collisions with buffer gas molecules.[22] Ion CCS measurements have also been realized in ion cyclotron resonance cells (ICR) in vacuum environments through measuring the line width of mass peaks in a mass spectrum.[22]

Capable of performing mass analysis and tandem MS, ion traps have been widely used in MS instruments, especially in hybrid MS instruments.[23-26] The electric field within a practical quadrupole ion trap can be expressed as a summation of quadrupole electric field and high-order electric fields.[27] Although high-order electric fields would normally cause mass resolution degradation[28] and chemical mass shifts,[29-31] they are inevitable[32] and introduced by electrode truncation,[33] geometry deviation,[34] space charge effects[35, 36] and etc.. On the other hand, proper use of high-order electric fields could enhance the performances of an ion trap, such as the nonlinear ion resonance ejection in high capacity ion traps (HCT, Bruker Corporation) and ion traps with simplified geometries.[37]

In this study, high-order electric fields were added into a linear ion trap on purpose, and a time-frequency analysis method was proposed to measure the CCS of an ion within the ion trap. Previous studies have shown that even-order electric fields would cause ion motion frequency shift, which depends on ion motion amplitude. At the same time, ion motion amplitude would decay due to ion-neutral collisions, in which the collision probability is a function of ion CCS. With these in mind, a relationship between ion motion frequency shift and ion CCS was established and utilized to measure ion CCSs through time-frequency analyses of ion trajectories in the linear ion trap (or ion motion induced image current[38-42]). Theoretical results were verified by number simulations, and calculation of the CCSs of bradykinin, angiotensin I/II and ubiquitin ions were demonstrated, including the identification of ubiquitin isomer ions.

2. Theory

In an ideal quadrupole ion trap (100% quadrupole electric field), ion motion frequency is independent of ion motion amplitude. In a practical system, ions trapped within a quadrupole ion trap could be affected by high-order electric fields, which will result in nonlinear resonances[43-46] and "mass shift". Theoretical analyses have shown that even-order fields may lead to ion motion frequency shifts, while odd-order fields lead to ion motion center displacements.[37] Besides high-order fields, ion motion could also be affected by ion-neutral collisions.[47] When considering both effects, ion-neutral collisions will induce ion motion amplitude decay, and reduced ion motion amplitude will lead to ion motion frequency shift with the presence of high-order fields. Therefore, the relationship between ion CCS and ion motion frequency could be established.

The electric potential (Φ) in a linear ion trap can be written as a weighted summation of high order fields,[48]

$$\phi = [U - V\cos(\Omega t)]\left(A_2\frac{x^2-y^2}{\rho_0^2} + A_3\frac{x^3-3xy^2}{\rho_0^3} + A_4\frac{x^4-6x^2y^2+y^4}{\rho_0^4} + A_5\frac{x^5-10x^3y^2+5xy^4}{\rho_0^5} + A_6\frac{x^6-15x^4y^2+15x^2y^4-y^6}{\rho_0^6} + \cdots\right) \quad (1)$$

where U and V are the amplitudes of the applied DC and RF voltages; Ω is the angular frequency of the RF voltage; A_2, A_3, A_4, A_5 and A_6 are the dimensionless amplitudes of high-order fields (for instance, A_2 corresponds to quadrupole field and A_3 corresponds to hexapole field); x and y are the Cartesian coordinates; ρ_0 is the distance from trap center to x- or y-electrode.

With the pseudo-potential approximation,[49] a differential equation based on

Newton's second law can be constructed. Ignoring odd-order fields, ion motion equation can then be expressed as,

$$u'' = -\omega_0^2\left(u + \frac{8A_2A_4}{{A_2}^2\rho_0^2}u^3 + \frac{6(2{A_4}^2+3A_2A_6)}{{A_2}^2\rho_0^4}u^5 + \ldots + F(A_{2n-2})u^{2n-1}\right) \quad (2)$$

where u could be either x or y, ω_0 is ion motion angular frequency in x- or y-direction. Although the pseudo-potential approximation is only accurate for $q < 0.4$ (in the Mathieu equation), it could give reasonable results for $q < 0.7$ in most cases. [50]

Solving Eqn. 2 with the harmonic balance method, the modified ion secular frequency (f) can be derived as, [51]

$$f = f_0\sqrt{1 + \frac{3a_1^2}{4}\epsilon_3 + \frac{5a_1^4}{8}\epsilon_5 + \frac{35a_1^6}{64}\epsilon_7 + \cdots} \quad (3)$$

where a_1 is ion motion amplitude, f_0 is ion secular frequency without considering high-order fields, ϵ_3, ϵ_5, ϵ_7 are coefficients representing the perturbations of even-order fields on ion motion.

When only octopole field is considered, the modified ion secular frequency can be written as,

$$f = f_0\sqrt{1 + \frac{3}{4}{a_1}^2\epsilon_3} \quad (4)$$

where $\epsilon_3 = \frac{8A_4}{A_2{\rho_0}^2}$.

When only dodecapole field is considered, the modified ion secular frequency becomes,

$$f = f_0\sqrt{1 + \frac{5}{8}{a_1}^4\epsilon_5} \quad (5)$$

where $\epsilon_5 = \frac{18A_6}{A_2{\rho_0}^4}$.

To take the ion-neutral collision effect into account, analytical expressions of ion motion trajectories with a realistic collision model need to be obtained first. Since the kinetic energy of an ion may vary significantly at different operation stages in an ion trap, the mixed collision model was used in this study. The mixed collision model was proposed as a combination of Langevin and hard-sphere collision models, where the collision probability is assumed to be a summation of an ion velocity independent term and an ion velocity dependent term.[52] With the mixed collision model, ion trajectory can be written as, [47]

$$a_1 = \frac{1}{(1/a_0+c)e^{\frac{\delta_1}{2}t}-c} \tag{6}$$

where α_0 is ion initial displacement or motional amplitude and $c = \frac{8\delta_2\omega_0}{3\pi\delta_1}$; $\delta_1 = \frac{q\sqrt{\frac{\alpha_p(M+m)}{mM}}}{2\varepsilon_0}\frac{p}{Tk}\frac{M}{m+M}$ is the Langevin damping coefficient; $\delta_2 = \sigma_{\text{hard-sphere}}\frac{p}{Tk}\frac{M}{m+M}$ is the hard-sphere damping coefficient and $\sigma_{\text{hard-sphere}} = \pi r_0^2$ is the collision cross section, where r_0 is the effective radius of the ion; q is the electric charge numbers of the ion; α_p is the polarizability of the buffer gas; ε_0 is the permittivity of vacuum; p is the pressure of the buffer gas; T is temperature; k is the Boltzmann constant; M is the mass of the buffer gas and m is the mass of the ion.

Substituting Eqn. 6 into Eqn. 4 or 5 (depends on which high-order field was added), a direct relationship between ion secular frequency and ion effective radius (r_0) could be set up. For example, when octopole field was applied, we could have,

$$f = f_0\sqrt{1+\frac{3}{4}\epsilon_3\left((1/a_0+c)e^{\frac{\delta_1}{2}t}-c\right)^{-2}} \tag{7}$$

As shown in Eqn. 7, ion secular frequency is changing with time with the presence of octopole field (with an example shown in Figure 1a). Since c is a function of ion hard-sphere CCS ($\sigma_{\text{hard-sphere}}$), ion CCSs could be calculated after knowing the ion secular frequency variations with respect to time, which can be done by performing time-frequency analysis on the ion trajectory (or the image currents collected from experiments). After rewriting, the relationship between f and r_0 can be written as,

$$f = f_0 \sqrt{1 + \frac{3}{4}\epsilon_3 \left(1/a_0\, e^{\frac{\delta_1}{2}t} + \left(e^{\frac{\delta_1}{2}t} - 1\right)\frac{8\omega_0}{3\delta_1}\frac{p}{Tk}\frac{M}{m+M} r_0^2\right)^{-2}} \qquad (8)$$

Figure 1a shows a typical the time-frequency mass spectrum after time-frequency analysis of an ion trajectory. Therefore, to perform experiments, the linear ion trap should have the capability of collecting ion image currents.[25]

A schematic process to determine ion CCSs from ion motion frequency was given in Figure 1b, 1c and 1d. As plotted in Figure 1b, ions with the same m/z ratio but different collision cross sections/effective radiuses would have different trajectories, specifically the ion with larger physical size decays faster than the other ion under the same condition. The left figure in Figure 1d shows the ion motion frequency curves versus time (namely ion time-frequency curves) for these two ions, which were obtained by applying the short time Fourier transform[53] (STFT) on ion trajectories. The frequency shift at time zero is the same for both ions, since both ions have the same initial condition. For the large ion (with faster ion motion amplitude decay in Figure 1b), its motion frequency will quickly converge to its secular frequency (f_0 in Eqn. 7). Ion motion frequency of the small ion would also converge to the same secular frequency (f_0), but with a slower speed. This convergence speed could be used to characterize ion CCSs (the left Figure 1d inset figure). To that end, a straight line was plotted to connect the starting point and the ending point of ion motion frequency, and the area (S) between ion time-frequency curve and this straight line could be used to quantify this convergence speed. The right figures in Figure 1d plot the frequency difference (*df*) between ion motion frequency and the straight line versus time (namely, *df*-versus-*t* curve). Finally, this area, *S*, could be translated back to ion collision cross sections/effective radiuses using Eqn.8. As shown in Figure 1c, a one-to-one relationship could be built between this area (*S*) and ion radius (r_0), when all other parameters were kept the same, including m/z of ions and ion trap operating conditions. The gradient of the *S*-versus-r_0 curve relates to the ion CCS measurement resolution, and a more accurate CCS could be obtained at the steeper region of the curve as indicated in Figure 1c.

3. Numerical Simulation

To validate theoretical results, simulation experiments were performed using a home-developed ion trajectory simulator which was coded in MATLAB (The MathWorks Inc. USA).[51, 54, 55] Ion motion differential equation was solved by the 5th-order Runge-Kutta integration method. The variation of ion frequency with respect to time was analyzed by the Fast Fourier Transform (FFT) and STFT. A realistic collision model, which combines the Langevin's collision model and the hard-sphere collision model, was used to calculate the collision probability in the simulation program.[47] Elastic collision model was applied to calculate the energy transfer between the ion neutral collision pair.

The linear ion trap used in this study has dimensions of $x_0 = y_0 = 5$ mm (center to electrode distance) and the RF trapping field was the summation of quadrupole field with either octopole field or dodecapole field. Following are the operation parameters (otherwise specified): the RF signal applied on the ion trap had a frequency of 1 MHz and amplitude of 400 $V_{0\text{-}p}$; ion initial displacement $\alpha_0 = 3$ mm; temperature was set at 300 K; Helium was used as the buffer gas (1 mTorr); ion trajectories was simulated for 5 ms. Ubiquitin (with +7 charges, +9 charges), bradykinin and angiotensin I/II were used as model ions in this simulation.

4. Results and Discussions

4.1 Parameter optimization

Instrument parameters of the ion trap were first optimized, including the percentage of high-order electric fields (octopole and/or dodecapole fields) and buffer gas pressure. Angiotensin II (m/z 524, ion effective radius 0.883 nm[56]) was used in the optimization process.

High-order electric field. High-order electric field is the key factor in ion CCS measurement, which induces ion motion frequency shift with respect to time. However, high-order electric fields may also cause degradation of mass resolution and mass shift. Therefore, percentages of high-order electric fields should be carefully controlled. To characterize the effects of high-order electric fields, controlled percentage of either octopole or dodecapole field (from -10% to +10%) was added into the linear ion trap for a comparison study. As shown in Figure 2, an octopole electric field would generally induce larger ion motion frequency shifts than a dodecapole field. Furthermore, the convergence speed of the ion motion frequency is faster with an added dodecapole field, since a dodecapole field will have much less field strength toward the center of the ion trap.[48] To have a long enough ion motion signal with frequency shift, octopole field is chosen over dodecapole field. A negative octopole field is then determined, since negative high-order field would induce more ion motion frequency shift as shown in Eqn. 4, as well as in Figure 2b and 2d. Furthermore, it has been shown that ion ejection resolution could be enhanced with added negative octopole fields.[57] Finally a -3% octopole electric field was chosen as the high-order fields in the linear ion trap, which is a compromise between octopole field induced ion instability and a large enough ion motion frequency shift.

Buffer gas. Helium and nitrogen are normally used as the buffer gases in quadruple ion traps.[58, 59] Since nitrogen is 7 times heavier than helium and the molecular polarizability of nitrogen (1.7403×10^{-24} cm^3) is approximate 8 times that of helium (0.2051×10^{-24} cm^3), so nitrogen is expected to have a stronger damping effect on ion motions (Figure 3a). Under low pressure conditions (10^{-5} Torr) and using helium as the buffer gas, the attenuation coefficient of ion motion amplitude is small (Figure 3b). To have large enough ion motion frequency shift for ion CCS calculation (measurable area S Figure 3c), it is necessary to extend image current collection duration. On the other extreme, under high pressure conditions (10^{-3} torr) and using nitrogen as the buffer gas, ion motion frequency shift would happen in a much shorter time (Figure 3b). However, shorter time also causes lower frequency resolution in a FT analysis process. Furthermore, the CCSs of ions also vary significantly, for example, the radius of a protein ion is on the level of 1~8 nm, while on the level of < 2.5 nm for a small peptide. The operating conditions should be optimized for different types of ions to make sure there is enough time to collect the ion motion signal (5 ms for instance) for accurate time-frequency analysis. In general, high mass buffer gas and/or high pressure should be used for protein ions, while low mass gas and/or low pressure can be applied for small ions. For the ions analyzed in this work (r_0 varies from 0.8 nm to 2.3 nm, and m/z is below 1250 Da), helium at 1 mTorr could be used as the buffer gas, where ion CCS measurements could achieve reasonable resolutions at the steeper region of the S-versus-r_0 curve (Figure 3d).

To maximize both mass resolution and resolving power in determining ion CCSs, operation parameters of the ion trap were optimized, including the effects of q value and the ion excitation mode.

q value. q value is an important parameter during the operation of an ion trap, which determines ion secular frequency. High-order fields induced ion motion frequency shift is also a function of q value. At q values of 0.3 and 0.6, the ion motion frequency shift at time zero is 105.754 KHz and 211.518 KHz, respectively. However, since the theoretical results (Eqn. 7) would be more accurate at lower q values, as well as to avoid nonlinear resonance points at high q regions (Figure 4a), it is suggested that the ion trap should work at low q regions (< 0.4) when performing ion CCS measurement. Due to the non-destructive nature of image current measurements, the proposed ion CCS measurement could be carried out before a dipolar resonance ejection. Therefore, the dipolar resonance ejection could also be performed at high q regions for optimized mass resolution.

Ion excitation mode. To experience the high-order field induced frequency shift, as well as for image current detection, ions need to be excited to a larger radius before performing CCS measurements. There are two ion excitation modes, the broadband ion excitation and the narrow band ion excitation. In the broadband ion excitation mode, ions within a mass range were excited simultaneously using a broadband AC waveform, such as a short duration DC pulse or a stored waveform inverse Fourier transform waveform (SWIFT).[60-62] Ions with different m/z ratios could be excited to the same radius or different radiuses, which can be controlled by adjusting the power distribution within the SWIFT waveform. With broadband ion excitation, all excited ions would experience the same RF voltage, thus different q values. Therefore, different ions would have different S-versus-r_0 curves. As an example, four ions with m/z 250 Da, 500 Da, 1000 Da and 2000 Da were placed in the linear ion trap with a 400 $V_{0\text{-}p}$ RF signal applied. These four ions would be trapped at q values of 0.6258, 0.3129, 0.1565, 0.0782, respectively. After excited to the same radius (3 mm), the S-versus-r_0 curves for these four ions were generated and plotted in Figure 4b. A steeper range exists in the low ion radius range for ions with low m/z ratios, ~ 0.4 nm to 1.6 nm for the ion with a m/z ratio 250 Da, for instance. For ions with larger m/z ratios, the steeper range lies in a bigger ion radius range, ~ 2.0 nm to 8.0 nm for the ion with a m/z ratio 2000 Da. Since ions with larger m/z ratios would typically have bigger ion radiuses, results suggest that the broadband excitation and detection method would be a fast and reasonable approach for CCS measurements for ions within a mass range.

In the narrow band excitation mode, ions with different m/z ratios could be excited and have their CCSs measured one-after-another at the same q value. As shown in Figure 4c, the S-versus-r_0 curves were generated at the same q value (0.3) for these four ions (m/z 250 Da, 500 Da, 1000 Da and 2000 Da). In this case, the S-versus-r_0 curves have a similar trend, while large ions would have a relatively wider steep range. In this mode, optimized q values could be selected for ions with different m/z ratios for maximized CCS resolving power.

4.2 Simulation results of ion CCS measurements

Broadband measurement. With the broadband ion excitation and detection, trajectories of four ions were simulated, including angiotensin I (+3 ion, m/z 433 Da, r_0 1.022 nm), angiotensin II (+2 ion, m/z 524 Da, r_0 0.883 nm), bradykinin (+1 ion, m/z 1060.2 Da, r_0 0.883 nm) and ubiquitin (+9 ion, m/z 952 Da, r_0 2.291 nm). In the simulation, ions were all excited to 3 mm; RF voltage was set at 400 $V_{0\text{-}p}$, 1 MHz; Helium was used as the buffer gas, 1 mTorr; image current was collected for 5 ms. Figure 5a shows the time-frequency mass spectra of these four ions. After analyzing the frequency shift, the *df*-versus-*t* curves could be generated (the solid lines in Figure 5b). The *df*-versus-*t* curves generated from simulated ion trajectory agree well with those calculated from theoretical calculations (the dashed lines in Figure 5b). Jittering of the *df*-versus-*t* curves in simulation results (Figure 5b) might be due to the random nature of ion-neutral collisions in simulation. Simulation was repeated five times, and the calculated CCSs were shown in Table 1 and Figure 5c. Ion CCSs measured with this time-frequency analysis method agree well with the CCS values (taken from ion mobility measurements).[56, 63, 64] When experiments were performed, many other factors would degrade the performance of this time-frequency analysis method, such as the noise level in the image current detection circuit, space charge effects, ion fragmentation and etc.

Sample	r_0(nm) from IMS*	Calculated r_0(nm)	Relative error(%)
angiotensin I	1.022	0.972±0.054	-4.84
angiotensin II	0.883	0.840±0.063	-4.94

bradykinin	0.883	0.867±0.085	-1.78
+9 ubiquitin	2.291	2.172±0.051	-5.21

Table 1. CCSs obtained from time-frequency analysis of trajectory simulations.

Note *: radius r_0 was calculated using $s = \pi r_0^2$, s the CCS from IMS results.

Analysis of isomer ions. The identification of isomer ions is an important task in ion structure analysis, especially for biomolecules (such as proteins) which would have different conformations. By analyzing the CCSs of ions besides m/z ratios, isomer ions could be resolved using the time-frequency analysis method. As a demonstration, the two isomers of ubiquitin ions with +7 charges (*m/z* 1224 Da, r_0 2.047 nm for one isomer, r_0 2.243 nm for the other isomer)[64] were studied through ion trajectory simulations followed by the time-frequency analyses. A q value of 0.1278 was used in the simulation for these isomer ions. As shown in Figure 6a and 6b, these two isomer ions would have the same ion secular frequency with the same ion motion amplitude. With different ion-neutral collision rates, isomer ions could be differentiated in the time-frequency spectrum (Figure 6a). Thus, their corresponding *df*-versus-*t* curves were also different as shown in Figure 6b. The CCSs of these two ubiquitin ions obtained from simulations were shown and compared with theoretical values[64] in Table 2 and Figure 6c.

Sample	r_0(nm) from IMS	Calculated r_0(nm)	Relative error(%)
+7 ubiquitin small isomer	2.047	1.911±0.050	-6.67
+7 ubiquitin large isomer	2.243	2.085±0.105	-7.01

Table 2. CCSs obtained from time-frequency analysis of trajectory simulations for ubiquitin ions with +7 charges.

4.3 Practical considerations in experiments

Control of high-order fields. Accurately control the percentage of high-order fields is one of the most important parameters in this method. A larger percentage of high-order electric field will increase ion motion frequency shift and help improve ion CCSs measurement resolution. On the other hand, larger high-order electric field also leads to reduced m/z resolution and instability regions in the stability diagram of an ion trap. A precise control of the high-order fields depends on machining and assembly accuracy of the ion trap,[65] as well as surface roughness.[34] In a practical mass spectrometry system, a calibration sample with given CCS can be used to calculate the percentage of the high-order fields (according to Equ.8) in the fabricated ion trap before testing unknown samples.

Image current signal processing. In order to calculate the CCS of an ion accurately from the image current, a time-frequency curve with high resolution in both time and frequency domain is required. However, there is typically a tradeoff for obtaining high resolutions in both time domain and frequency domain. STFT is a straight forward time-frequency analysis method, and other methods could be tested in the future to improve the resolutions.[66-68] On the other hand, the time-frequency curve will be "truncated" at both ends, since a finite length of time domain signal (the size of the window for STFT) is required to generate a frequency data point (Figure 5b and

6b). As a result, the calculated area S is expected to be smaller due to the lack of frequency data points at the beginning and end of the time-frequency curves. A system error will then be introduced, and the calculated ion radii/CCSs from this method would be smaller than the theoretical ion radii/CCSs (Figure 5c and 6c). Furthermore, electrical and chemical noises exist in the image current signal measured from a practical ion trap, which were not considered in the simulation. Gaussian noise and the coupling of rf signal on the image current detection circuit are the major sources of electrical noises,[69] which will degrade ion CCS measurement and need to be minimized. Chemical noises could be avoided by isolating ions of interest before performing the CCS measurement.

Difference between IMS results and CCS measured in ion trap. Typically an IMS operates at a much higher pressure than that in a quadrupole ion trap.[70] Therefore, the CCS measurement results might be different from that obtained from a quadrupole ion trap using the method proposed in this work. The CCS measurements at a much lower pressure has been demonstrated in FT-ICR cells, and those results do not overlap but show linear correlation with IMS results.[22] In addition, ion-neutral collision energies and collision models are also different in IMS, ion traps and FTICR cells, which might also contribute to the differences in CCS measurement results. It is also believed that the CCS results from this method would also have linear correlation with those from IMS measurements, but not necessarily equal to each other.

5. Conclusion

A proof-of-concept, time-frequency analysis technique for determining ion CCSs via analyzing the ion trajectories (or ion image currents) in quadrupole ion traps was demonstrated theoretically, and verified by simulations. With the mixed collision models and the pseudo-potential approximation, analytical expressions of modified ion secular frequency in a linear ion trap were obtained using the harmonic balance method. Based on theoretical derivation, df-versus-t and S-versus-r_0 curves could be used to calculate ion CCSs. The CCS measurements of ubiquitin, bradykinin, angiotensin I and II were simulated, and a relative error within ~6% could be achieved in simulations under optimized conditions. Isomer ions of ubiquitin could also be distinguished. As a complementary ion structure analysis technique, this time-frequency based ion CCS measurement method would add new capabilities to quadrupole ion traps. Further researches are highly demanded to realize this method in experiments.

Acknowledgements

This work was supported by NNSF China (21205005, 21475010), "1000 plan" in China, MOST instrumentation program of China (2011YQ09000502, 2011YQ09000501 and 2012YQ040140-07) and National vacuum and physics laboratory (ZDK1401).

References

1. Cooks, R. G., Special feature: Historical. Collision‐induced dissociation: Readings and commentary. *Journal of Mass Spectrometry* 1995, 30, 1215-1221.
2. Dodds, E. D.; German, J. B.; Lebrilla, C. B., Enabling MALDI-FTICR-MS/MS for high-performance proteomics through combination of infrared and collisional activation. *Anal. Chem.* 2007, 79, 9547-9556.
3. March, R. E.; Todd, J. F. J., *Quadrupole Ion Trap Mass Spectrometry*. 2nd edition ed.; John Wiley & Sons Inc.: Hoboken, New Jersey, 2005.
4. Coon, J.; Shabanowitz, J.; Hunt, D.; Syka, J. P., Electron transfer dissociation of peptide anions. *J Am Soc Mass Spectrom* 2005, 16, 880-882.
5. Huzarska, M.; Ugalde, I.; Kaplan, D. A.; Hartmer, R.; Easterling, M. L.; Polfer, N. C., Negative Electron Transfer Dissociation of Deprotonated Phosphopeptide Anions: Choice of Radical Cation Reagent and Competition between Electron and Proton Transfer. *Anal. Chem.* 2010, 82, 2873-2878.
6. Vincent, C. E.; Rensvold, J. W.; Westphall, M. S.; Pagliarini, D. J.; Coon, J. J., Automated Gas-Phase Purification for Accurate, Multiplexed Quantification on a Stand-Alone Ion-Trap Mass Spectrometer. *Anal. Chem.* 2012, 85, 2079-2086.
7. Kalli, A.; Sweredoski, M. J.; Hess, S., Data-Dependent Middle-Down Nano-Liquid Chromatography-Electron Capture Dissociation-Tandem Mass Spectrometry: An Application for the Analysis of Unfractionated Histones. *Anal. Chem.* 2013, 85, 3501-3507.
8. Mikhailov, V. A.; Iniesta, J.; Cooper, H. J., Top-Down Mass Analysis of Protein Tyrosine Nitration: Comparison of Electron Capture Dissociation with "Slow-Heating" Tandem Mass Spectrometry Methods. *Anal. Chem.* 2010, 82, 7283-7292.
9. Xu, F. M.; Xu, Q. G.; Dong, X. T.; Guy, M.; Guner, H.; Hacker, T. A.; Ge, Y., Top-down high-resolution electron capture dissociation mass spectrometry for comprehensive characterization of post-translational modifications in Rhesus monkey cardiac troponin I. *Int. J. Mass Spectrom.* 2011, 305, 95-102.
10. Garcia, B. A.; Siuti, N.; Thomas, C. E.; Mizzen, C. A.; Kelleher, N. L., Characterization of neurohistone variants and post-translational modifications by electron capture dissociation mass spectrometry. *Int. J. Mass Spectrom.* 2007, 259, 184-196.
11. de Carvalho, R. V.; Lopez-Ferrer, D.; Guimaraes, K. S.; Lins, R. D., IMSPeptider: A computational peptide collision cross-section area calculator based on a novel molecular dynamics simulation protocol. *J. Comput. Chem.* 2013, 34, 1707-1718.
12. Pagel, K.; Harvey, D. J., Ion Mobility-Mass Spectrometry of Complex Carbohydrates: Collision Cross Sections of Sodiated N-linked Glycans. *Anal. Chem.* 2013, 85, 5138-5145.
13. Shimizu, A.; Chiba, M., Ion Mobility Spectrometry-Mass Spectrometry Analysis for the Site of Aromatic Hydroxylation. *Drug Metab. Dispos.* 2013, 41, 1295-1299.
14. Pringle, S. D.; Giles, K.; Wildgoose, J. L.; Williams, J. P.; Slade, S. E.; Thalassinos, K.; Bateman, R. H.; Bowers, M. T.; Scrivens, J. H., An investigation of the mobility separation of some peptide and protein ions using a new hybrid quadrupole/travelling wave IMS/oa-ToF instrument. *International Journal of Mass Spectrometry* 2007, 261, 1-12.
15. Fenn, L.; Kliman, M.; Mahsut, A.; Zhao, S.; McLean, J., Characterizing ion mobility-mass spectrometry conformation space for the analysis of complex biological samples. *Anal Bioanal Chem* 2009, 394, 235-244.

16. Fernandez-Lima, F. A.; Blase, R. C.; Russell, D. H., A study of ion-neutral collision cross-section values for low charge states of peptides, proteins, and peptide/protein complexes. *International Journal of Mass Spectrometry* 2010, 298, 111-118.
17. Dilger, J.; Valentine, S.; Glover, M.; Clemmer, D., A Database of Alkaline-Earth-Coordinated Peptide Cross Sections: Insight into General Aspects of Structure. *J. Am. Soc. Mass Spectrom.* 2013, 24, 768-779.
18. Clemmer, D. E.; Jarrold, M. F., Ion mobility measurements and their applications to clusters and biomolecules. *Journal Of Mass Spectrometry* 1997, 32, 577-592.
19. Blagojevic, V.; Bohme, D. K., Trimethylation and Differential Mobility Spectroscopy in Quantitative Peptide Analysis: Increasing Selectivity and Sensitivity through Ion/Molecule Chemistry. *ChemPlusChem* 2013, 78, 1049-1052.
20. Guevremont, R., High-field asymmetric waveform ion mobility spectrometry: A new tool for mass spectrometry. *Journal Of Chromatography A* 2004, 1058, 3-19.
21. Shvartsburg, A. A.; Smith, R. D., Fundamentals of Traveling Wave Ion Mobility Spectrometry. *Anal. Chem.* 2008, 80, 9689-9699.
22. Yang, F.; Voelkel, J. E.; Dearden, D. V., Collision Cross Sectional Areas from Analysis of Fourier Transform Ion Cyclotron Resonance Line Width: A New Method for Characterizing Molecular Structure. *Anal. Chem.* 2012, 84, 4851-4857.
23. Hager, J. W., A new linear ion trap mass spectrometer. *Rapid Communications In Mass Spectrometry* 2002, 16, 512-526.
24. Myung, S.; Lee, Y. J.; Moon, M. H.; Taraszka, J.; Sowell, R.; Koeniger, S.; Hilderbrand, A. E.; Valentine, S. J.; Cherbas, L.; Cherbas, P.; Kaufmann, T. C.; Miller, D. F.; Mechref, Y.; Novotny, M. V.; Ewing, M. A.; Sporleder, C. R.; Clemmer, D. E., Development of high-sensitivity ion trap ion mobility spectrometry time-of-flight techniques: A high-throughput nano-LC-IMS-TOF separation of peptides arising from a Drosophila protein extract. *Anal. Chem.* 2003, 75, 5137-5145.
25. Douglas, D. J.; Frank, A. J.; Mao, D. M., Linear ion traps in mass spectrometry. *Mass Spectrometry Reviews* 2005, 24, 1-29.
26. Makarov, A.; Denisov, E.; Kholomeev, A.; Baischun, W.; Lange, O.; Strupat, K.; Horning, S., Performance evaluation of a hybrid linear ion trap/orbitrap mass spectrometer. *Anal. Chem.* 2006, 78, 2113-2120.
27. Smythe, W. R., *Static and dynamic electricity*. McGraw-Hill: 1950.
28. Makarov, A. A., Resonance Ejection from the Paul Trap: A Theoretical Treatment Incorporating a Weak Octapole Field. *Anal. Chem.* 1996, 68, 4257-4263.
29. Li, H.; Plass, W. R.; Patterson, G. E.; Cooks, R. G., Chemical mass shifts in resonance ejection experiments in the quadrupole ion trap. *Journal of Mass Spectrometry* 2002, 37, 1051-1058.
30. Wells, J. M.; Plass, W. R.; Cooks, R. G., Control of Chemical Mass Shifts in the Quadrupole Ion Trap through Selection of Resonance Ejection Working Point and rf Scan Direction. *Analytical Chemistry* 2000, 72, 2677-2683.
31. Li, H. Y.; Peng, Y. N.; Plass, W. R.; Cooks, R. G., Chemical mass shifts in quadrupole ion traps as analytical characteristics of nitro-aromatic compounds. *Int. J. Mass Spectrom.* 2003, 222, 481-491.
32. Lammert, S. A.; Plass, W. R.; Thompson, C. V.; Wise, M. B., Design, optimization and initial performance of a toroidal rf ion trap mass spectrometer. *Int. J. Mass Spectrom.* 2001, 212, 25-40.
33. Beaty, E. C., CALCULATED ELECTROSTATIC PROPERTIES OF ION TRAPS. *Physical Review A* 1986, 33, 3645-3656.
34. Xu, W.; Chappell, W. J.; Cooks, R. G.; Ouyang, Z., Characterization of electrode surface roughness

and its impact on ion trap mass analysis. *Journal Of Mass Spectrometry* 2009, 44, 353-360.

35. Vedel, F.; Andre, J.; Vedel, M.; Brincourt, G., COMPUTED ENERGY AND SPATIAL STATISTICAL PROPERTIES OF STORED IONS COOLED BY A BUFFER GAS. *Physical Review A* 1983, 27, 2321-2330.

36. Li, G. Z.; Guan, S. H.; Marshall, A. G., Comparison of equilibrium ion density distribution and trapping force in Penning, Paul, and combined ion traps. *J Am Soc Mass Spectrom* 1998, 9, 473-481.

37. Wang, Y. Z.; Huang, Z. J.; Jiang, Y.; Xiong, X. C.; Deng, Y. L.; Fang, X.; Xu, W., The coupling effects of hexapole and octopole fields in quadrupole ion traps: a theoretical study. *Journal Of Mass Spectrometry* 2013, 48, 937-944.

38. Hilger, R. T.; Wyss, P. J.; Santini, R. E.; McLuckey, S. A., Absorption Mode Fourier Transform Electrostatic Linear Ion Trap Mass Spectrometry. *Analytical Chemistry* 2013, 85, 8075-8079.

39. Xu, W.; Maas, J. B.; Boudreau, F. J.; Chappell, W. J.; Zheng, O. Y., Nondestructive Ion Trap Mass Analysis at High Pressure. *Anal. Chem.* 2011, 83, 685-689.

40. Goeringer, D. E.; Crutcher, R. I.; McLuckey, S. A., ION REMEASUREMENT IN THE RADIO-FREQUENCY QUADRUPOLE ION-TRAP. *Anal. Chem.* 1995, 67, 4164-4169.

41. Soni, M.; Frankevich, V.; Nappi, M.; Santini, R. E.; Amy, J. W.; Cooks, R. G., Broad-band Fourier transform quadrupole ion trap mass spectrometry. *Analytical chemistry* 1996, 68, 3314-3320.

42. Badman, E. R.; Patterson, G. E.; Wells, J. M.; Santini, R. E.; Cooks, R. G., Differential non-destructive image current detection in a fourier transform quadrupole ion trap. *Journal of mass spectrometry* 1999, 34, 889-894.

43. Makarov, A. A., Resonance ejection from the Paul trap: A theoretical treatment incorporating a weak octapole field. *Anal. Chem.* 1996, 68, 4257-4263.

44. Konenkov, N.; Londry, F.; Ding, C. F.; Douglas, D. J., Linear quadrupoles with added hexapole fields. *J Am Soc Mass Spectrom* 2006, 17, 1063-1073.

45. Dawson, P. H.; Whetten, N. R., Non-linear resonances in quadrupole mass spectrometers due to imperfect fields I. The quadrupole ion trap. *International Journal of Mass Spectrometry and Ion Physics* 1969, 2, 45-59.

46. Dawson, P. H.; Whetten, N. R., Non-linear resonances in quadrupole mass spectrometers due to imperfect fields: II. The quadrupole mass filter and the monopole mass spectrometer. *International Journal of Mass Spectrometry and Ion Physics* 1969, 3, 1-12.

47. He, M.; Guo, D.; Xiong, X.; Fang, X.; Xu, W., Realistic Modeling of Ion-neutral Collisions in Quadrupole Ion Traps. *submit in Journal of Mass Spectrometry* 2014.

48. Douglas, D. J., LINEAR QUADRUPOLES IN MASS SPECTROMETRY. *Mass Spectrometry Reviews* 2009, 28, 937-960.

49. Major, F. G.; Dehmelt, H. G., Exchange-collision technique for the rf spectroscopy of stored ions. *Physical Review* 1968, 170, 91.

50. Xu, W.; Chappell, W. J.; Ouyang, Z., Modeling of ion transient response to dipolar AC excitation in a quadrupole ion trap. *International Journal of Mass Spectrometry* 2011, 308, 49-55.

51. Guo, D.; Wang, Y.; Xiong, X.; Zhang, H.; Zhang, X.; Yuan, T.; Fang, X.; Xu, W., Space Charge Induced Nonlinear Effects in Quadrupole Ion Traps. *J. Am. Soc. Mass Spectrom.* 2014, 25, 498-508.

52. Guan, S.; Li, G.-Z.; Marshall, A. G., Effect of ion-neutral collision mechanism on the trapped-ion equation of motion: a new mass spectral line shape for high-mass trapped ions. *International journal of mass spectrometry and ion processes* 1997, 167, 185-193.

53. Gabor, D., Theory of communication. Part 1: The analysis of information. *Electrical Engineers - Part III: Radio and Communication Engineering, Journal of the Institution of* 1946, 93, 429-441.

54. Xiong, X.; Xu, W.; Fang, X.; Deng, Y.; Ouyang, Z., Accelerated Simulation study of space charge effects in quadrupole ion traps using GPU techniques. *Journal of the American Society for Mass Spectrometry* 2012, 23, 1799-1807.

55. Prentice, B. M.; Xu, W.; Ouyang, Z.; McLuckey, S. A., DC potentials applied to an end-cap electrode of a 3D ion trap for enhanced MSn functionality. *International Journal of Mass Spectrometry* 2011, 306, 114-122.

56. Bush, M. F.; Hall, Z.; Giles, K.; Hoyes, J.; Robinson, C. V.; Ruotolo, B. T., Collision Cross Sections of Proteins and Their Complexes: A Calibration Framework and Database for Gas-Phase Structural Biology. *Analytical Chemistry* 2010, 82, 9557-9565.

57. Zhang, Z. P.; Quist, H.; Peng, Y.; Hansen, B. J.; Wang, J. T.; Hawkins, A. R.; Austin, D. E., Effects of higher-order multipoles on the performance of a two-plate quadrupole ion trap mass analyzer. *Int. J. Mass Spectrom.* 2011, 299, 151-157.

58. Louris, J. N.; Amy, J. W.; Ridley, T. Y.; Cooks, R. G., Injection of ions into a quadrupole ion trap mass spectrometer. *International journal of mass spectrometry and ion processes* 1989, 88, 97-111.

59. Gao, L.; Sugiarto, A.; Harper, J. D.; Cooks, R. G.; Ouyang, Z., Design and characterization of a multisource hand-held tandem mass spectrometer. *Analytical chemistry* 2008, 80, 7198-7205.

60. Soni, M. H.; Cooks, R. G., Selective Injection and Isolation of Ions in Quadrupole Ion Trap Mass Spectrometry Using Notched Waveforms Created Using the Inverse Fourier Transform. *Anal. Chem.* 1994, 66, 2488-2496.

61. Guan, S.; Marshall, A. G., Stored waveform inverse Fourier transform axial excitation/ejection for quadrupole ion trap mass spectrometry. *Anal. Chem.* 1993, 65, 1288-1294.

62. Julian, R. K.; Cooks, R. G., Broad-band excitation in the quadrupole ion trap mass spectrometer using shaped pulses created with the inverse Fourier transform. *Anal. Chem.* 1993, 65, 1827-1833.

63. Wyttenbach, T.; vonHelden, G.; Bowers, M. T., Gas-phase conformation of biological molecules: Bradykinin. *Journal Of the American Chemical Society* 1996, 118, 8355-8364.

64. Valentine, S. J.; Counterman, A. E.; Clemmer, D. E., Conformer-dependent proton-transfer reactions of ubiquitin ions. *J Am Soc Mass Spectrom* 1997, 8, 954-961.

65. Wang, Y.; Zhang, X.; Feng, Y.; Shao, R.; Xiong, X.; Fang, X.; Deng, Y.; Xu, W., Characterization of geometry deviation effects on ion trap mass analysis: A comparison study. *International Journal of Mass Spectrometry* 2014, 370, 125-131.

66. Aushev, T.; Kozhinov, A. N.; Tsybin, Y. O., Least-Squares Fitting of Time-Domain Signals for Fourier Transform Mass Spectrometry. *J. Am. Soc. Mass Spectrom.* 2014, 25, 1263-1273.

67. Chou, S. W.; Shiu, G. R.; Chang, H. C.; Peng, W. P., Wavelet-Based Method for Time-Domain Noise Analysis and Reduction in a Frequency-Scan Ion Trap Mass Spectrometer. *J. Am. Soc. Mass Spectrom.* 2012, 23, 1855-1864.

68. Koo, I.; Zhang, X.; Kim, S., Wavelet- and Fourier-Transform-Based Spectrum Similarity Approaches to Compound Identification in Gas Chromatography/Mass Spectrometry. *Analytical Chemistry* 2011, 83, 5631-5638.

69. Xu, W.; Maas, J. B.; Boudreau, F. J.; Chappell, W. J.; Ouyang, Z., Nondestructive Ion Trap Mass Analysis at High Pressure. *Analytical Chemistry* 2010, 83, 685-689.

70. Eiceman, G. A.; Karpas, Z.; Hill, H. H., *Ion Mobility Spectrometry, Third Edition*. Taylor & Francis: 2013.

Figure 1

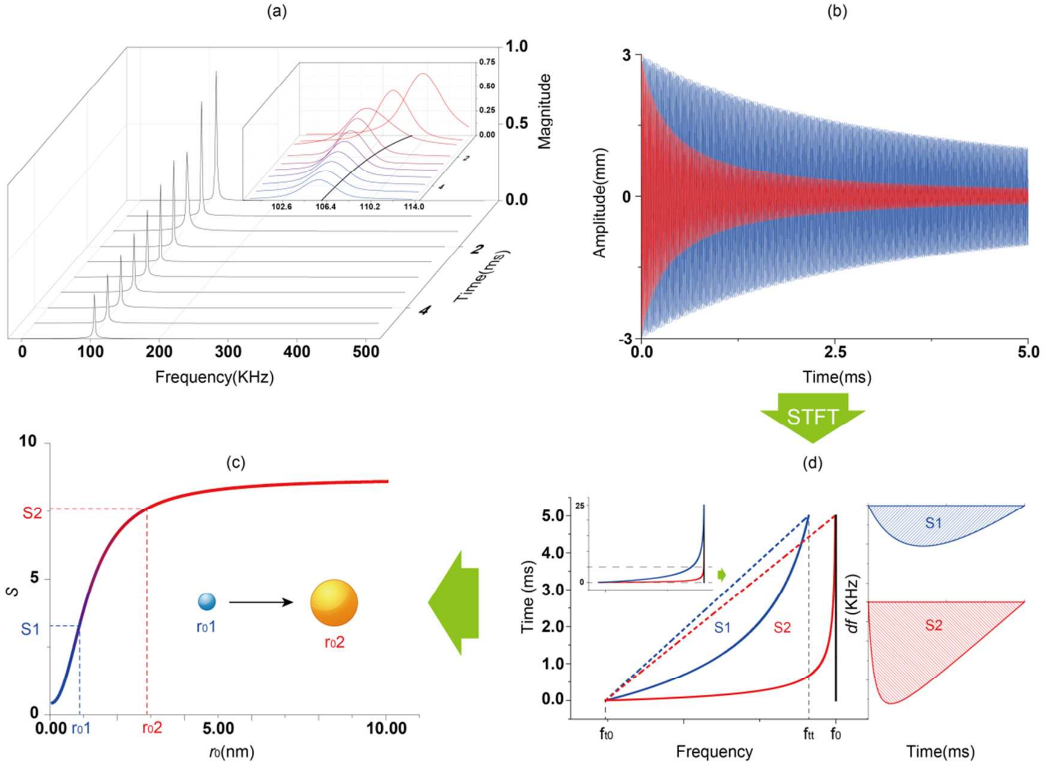

Figure 1. Schematic process of measuring ion CCSs using time-frequency analyses. (a) A typical time-frequency mass spectra in which ion secular frequency shift with time; (b) decayed ion trajectories for two ions with the same m/z but different CCSs; (c) the *S*-versus-r_0 curve; (d) ion time-frequency curves (left) and *df*-versus-*t* curves (right) for two isomers. See text for details.

Figure 2

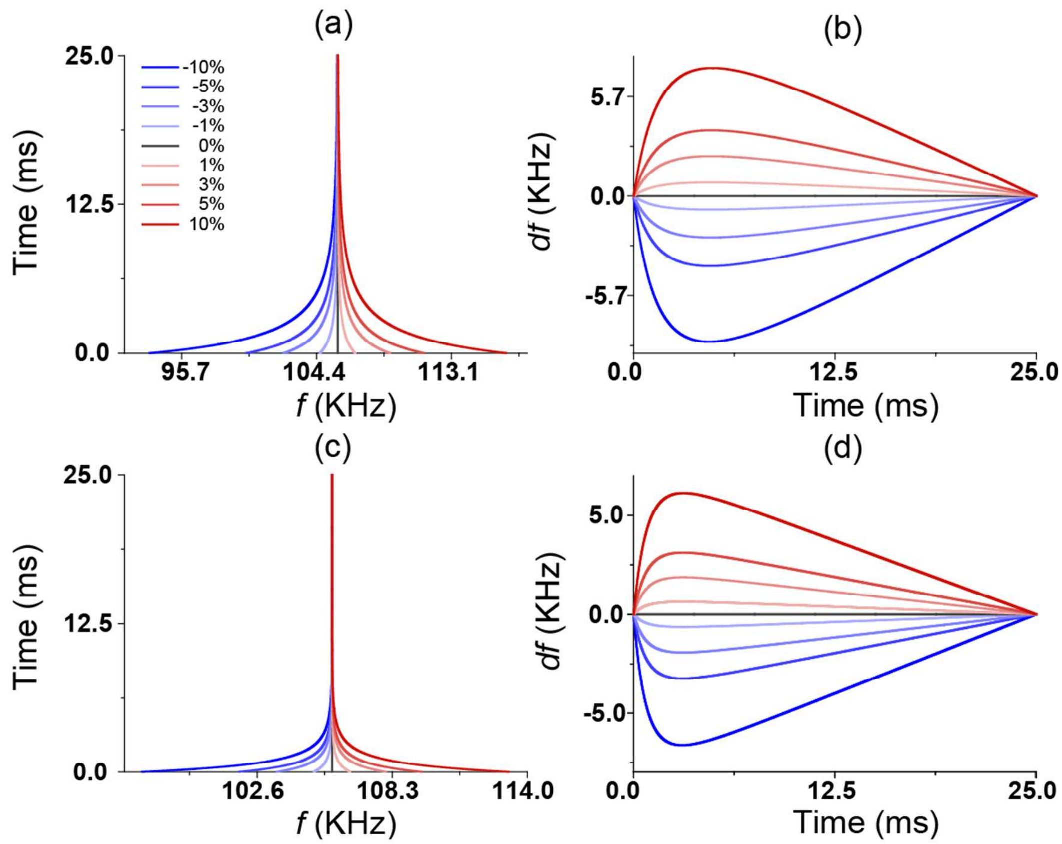

Figure 2. High-order field effects on ion motion frequencies. (a) ion time-frequency curves under different percentages of octopole fields; (b) ion *df*-versus-*t* curves under different percentages of octopole fields; (c) ion time-frequency curves under different percentages of dodecapole fields; (d) ion *df*-versus-*t* curves under different percentages of dodecapole fields. Angiotensin II with $r_0 = 0.883$ nm (CCS) and $m/z = 524$.

Figure 3

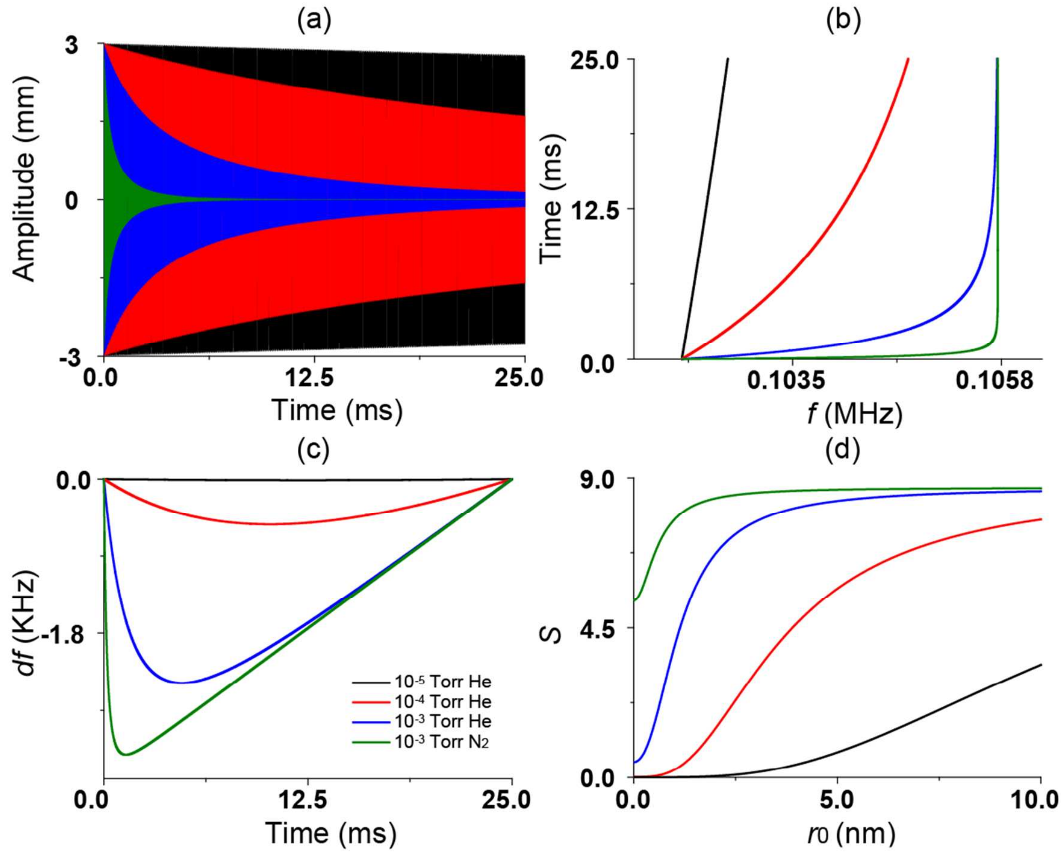

Figure 3. Buffer gas effects on ion CCS measurements using the time-frequency method. (a) ion damping processes with different buffer gases; (b) ion time-frequency curves with different buffer gases; (c) ion *df*-versus-*t* curves with different buffer gases; (d) ion *S*-versus-r_0 curves with different buffer gases. Angiotensin II with $r_0 = 0.883$ nm (CCS) and $m/z = 524$.

Figure 4

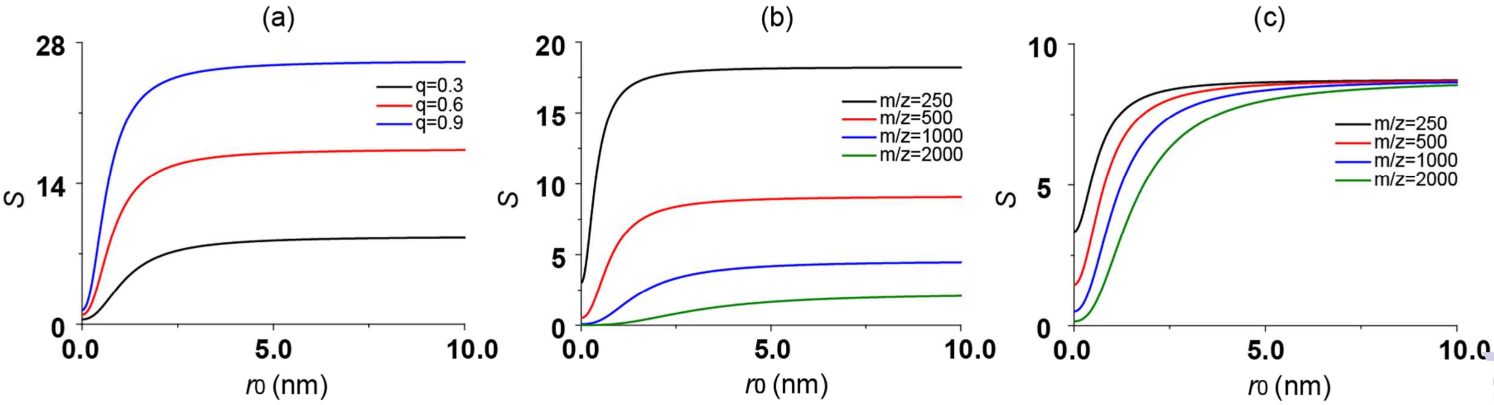

Figure 4. The S-versus-r_0 curves at different operating conditions. (a) Angiotensin II trapping at different q values; (b) different ions with ion trajectories acquired at the same rf voltage, 400 $V_{0\text{-}p}$ (broadband measurement); (c) different ions with ion trajectories acquired at the same q value, 0.3 (narrow band measurement).

Figure 5

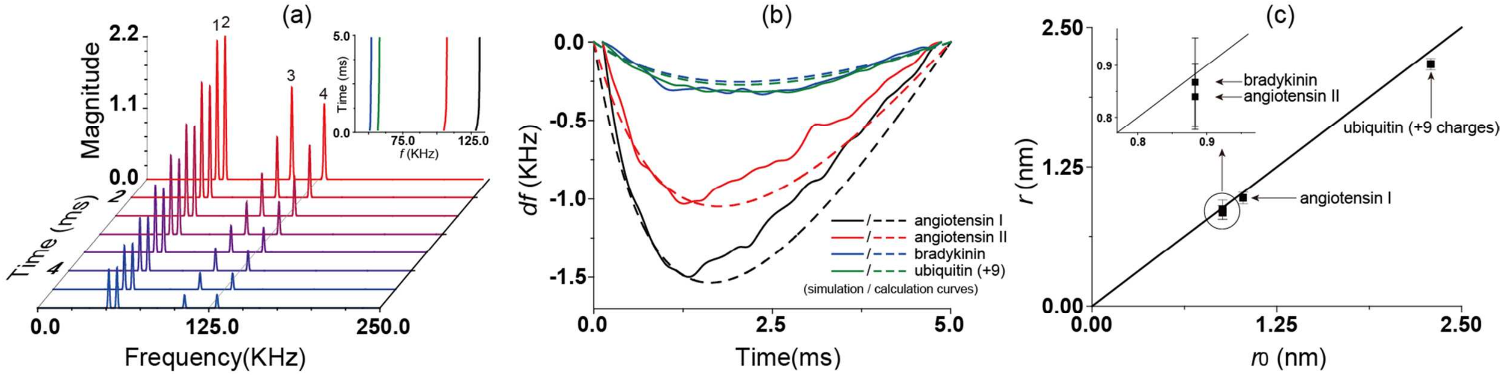

Figure 5. Measured ion CCSs from ion trajectory simulation. (a) Time-frequency mass spectra of 4 ions (1. bradykinin, 2. ubiquitin with +9 charges, 3. angiotensin II, 4. angiotensin I); (b) the corresponding *df*-versus-*t* curves by simulation (solid lines) and *df*-versus-*t* curves by theoretical calculation (dashed lines); (c) theoretical CCSs versus CCSs obtained from simulation.

Figure 6

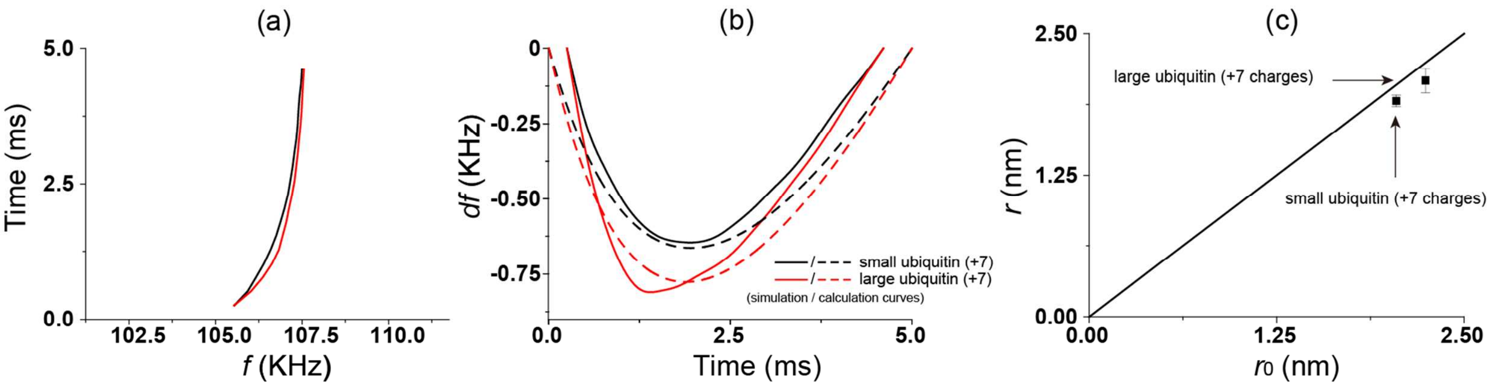

Figure 6. Analyses of isomers with the time-frequency method. (a) Simulated time-frequency curves of two isomers; (b) the corresponding *df*-versus-*t* curves by simulation (solid lines) and *df*-versus-*t* curves by theoretical calculation (dashed lines); (c) theoretical CCSs vs CCSs obtained from simulation. Ubiquitin with +7 charges and *m/z* =1224, the larger isomer r_0 = 2.047 nm and the smaller isomer r_0 = 2.243 nm.

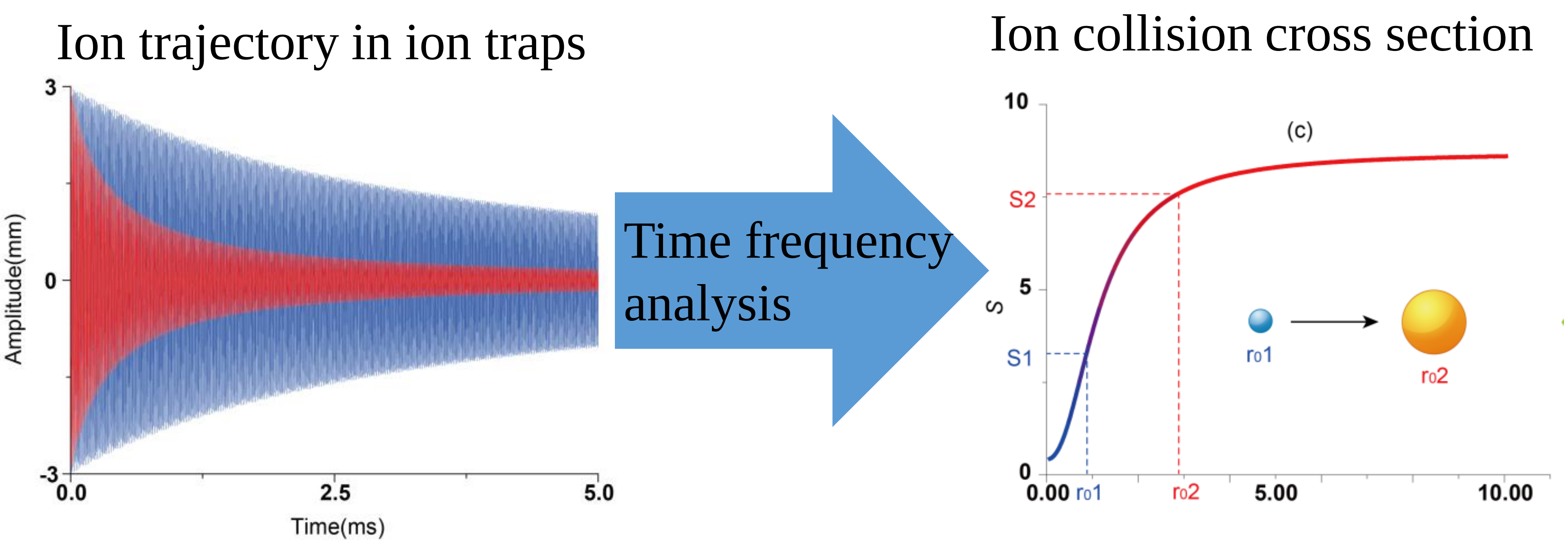
Ion trajectory in ion traps
3
0
-3
Amplitude(mm)
0.0
2.5
5.0
Time(ms)
Time frequency analysis
Ion collision cross section
10
(c)
S2
5
S
S1
0
0.00
r0 1
r0 2
5.00
10.00
r0 1
r0 2